ELSEVIER

Journal of Photochemistry and Photobiology A: Chemistry 91 (1995) 1–6

Journal of PHOTOCHEMISTRY AND PHOTOBIOLOGY A:CHEMISTRY

UV absorption cross-section data for the hypochlorites ROCl (R ≡ H, CH_3, C_2H_5, i-C_3H_7, tert-C_4H_9)

Tim P.W. Jungkamp, Ulf Kirchner, Mark Schmidt, Ralph N. Schindler

Institut für Physikalische Chemie, Universität Kiel, Ludewig-Meyn-Str. 8, 24098 Kiel, Germany

Received 25 July 1994; accepted 10 March 1995

Abstract

UV absorption cross-section data in the wavelength range 230 nm < λ < 400 nm are reported for the hypochlorites ROCl (R ≡ H, CH_3, C_2H_5, i-C_3H_7 or tert-C_4H_9). The data were obtained using a long-path UV absorption flow cell in a diode array spectrometer coupled to a quadrupole mass spectrometer with a molecular beam sampling inlet for purity control.

The absorption spectra of all the hypochlorites studied show a strong continuous band with a maximum around λ = 235–240 nm and a weak band centred at 310 nm. The alkyl substitution does not influence the spectral shape significantly. On the basis of this finding, it is suggested that the photochemical removal process for hypochlorites formed in the atmosphere will be the same as that of HOCl. The mass and IR absorption spectra of CH_3OCl are included as reference.

Keywords: UV Absorption; Hypochlorites; Diode array spectrometer

1. Introduction

Hypochloric acid (HOCl) is a temporary reservoir of atmospheric chlorine. Its formation in the stratosphere is attributed primarily to the homogeneous reaction between hydroperoxy radicals and ClO (Eq. (1)) and to the heterogeneous process (Eq. (2)) occurring in or on stratospheric clouds during the polar winter [1].

$$HO_2 + ClO \longrightarrow HOCl + O_2 \quad (1)$$

$$ClONO_2 + H_2O \longrightarrow HOCl + HNO_3 \quad (2)$$

Following the pioneering work of Reimann and Kaufmann [2] on the rate of the homogeneous HOCl formation reaction, several studies were carried out on the spectral properties of HOCl in the visible–near-UV [3–6] as well as on its photochemical removal processes [7–12]. On the basis of these early findings and kinetic studies on atmospheric HOCl destruction processes [13], it was concluded that the lifetime of HOCl in the atmosphere is primarily determined by its photolysis in the lower stratosphere [5]. This conclusion was reached long before the detection of HOCl in the atmosphere by far-IR emission studies [14] and IR absorption measurements [15]. Results from more recent laboratory experiments on the HOCl absorption spectrum and kinetic parameters for HOCl removal are given in Refs. [16–18].

In contrast with HOCl, until recently, very little attention had been paid to the involvement of the homologous hypochlorite CH_3OCl in the chemistry of the atmosphere. Crutzen et al. [19] pointed out that the initial build-up of RO_x would lead to enhanced HO_2 generation by a chain involving the methane oxidation cycle and would yield a more rapid ozone depletion. The reaction sequence

$$Cl + CH_4 + O_2 \longrightarrow CH_3O_2 + HCl \quad (3)$$

$$Cl + O_3 \longrightarrow ClO + O_2 \quad (4)$$

$$CH_3O_2 + OCl \longrightarrow CH_3OCl + O_2 \quad (5a)$$

$$CH_3O_2 + OCl \longrightarrow CH_3O + ClOO \quad (5b)$$

$$ClOO + M \longrightarrow Cl + O_2 \quad (6)$$

$$CH_3O + O_2 \longrightarrow HO_2 + HCHO \quad (7)$$

may be part of the depletion mechanism. In this sequence, reaction (5a) is analogous to step (1). It is tacitly assumed that CH_3OCl will eventually be converted to Cl_2 if the conversion occurs on PSC particles or will be decomposed photolytically in the stratosphere, similarly to HOCl, to yield CH_3O and Cl, as suggested by Helleis et al. [20].

Recent kinetic studies over a wide temperature range have shown that CH_3OCl is indeed an important product of reaction (5a) [20–22]. No data are available on the atmospheric degradation processes for methyl hypochlorite. To assess the

1010-6030/95/$09.50
SSDI 1010-6030(95)04074-9

role of the photochemical loss of CH_3OCl in the atmosphere, data on the absorption cross-section for this compound in the visible–near-UV range are required.

In this paper, gas phase absorption cross-sections are reported for the hypochlorites ROCl (R ≡ H, CH_3, C_2H_5, i-C_3H_7 and tert-C_4H_9) in the wavelength range 230 nm < λ < 400 nm. The spectra were obtained under flow conditions using a diode array spectrometer. The simultaneous recording of the mass spectra allowed trace impurities present in the gas flow to be identified. The mass and IR spectra of CH_3OCl are given as reference for kinetic studies.

2. Experimental details

2.1. Techniques

For UV measurements, a 42 cm double-wall Pyrex flow cell with quartz windows was employed. The cell could be cooled down to −60 °C. Its temperature was measured using calibrated thermocouples. The cell was equipped with a White system providing an effective path length of 3.36 m. Quartz fibre optics were used in the optical alignment. A Hamamatsu L 636 deuterium lamp served as light source. Using a double diode array system, intensity fluctuations of the light source were eliminated by registration in the double-beam mode. With a Jobin-Yvon HR 250 monochromator, the spectral range 230–400 nm was covered.

The cell was attached to an electron impact quadrupole mass spectrometer via a two-stage differential pumping system as described previously [18]. The ion source was operated at an electron energy of 30 eV.

Samples were transported through the cell with He as carrier gas at $p = 10$ mbar. The residence time in the cell was less than 3 s. Concentrations of HOCl were determined mass spectrometrically, calibrating the $HO^{35}Cl^+$ ion signal on mass 52 by titration of HOCl with F atoms [18]; additional consumption of F by H_2O and Cl_2O must be considered by numerical simulation of the reaction system. The concentrations of the other samples were determined by measuring the pressure drop in calibrated Pyrex volumes using MKS Baratron gauges.

The IR spectra of CH_3OCl samples were taken in the range 650–3200 cm^{-1} with a resolution of 0.25 cm^{-1}. A pressure of 0.5 mbar was used. The cell was equipped with a 40 m White system and attached to a Bruker IFS 66v FT spectrometer. A liquid-nitrogen-cooled HgCdTe detector was used.

2.2. Chemicals

Gaseous HOCl samples were obtained and transported into the cell by bubbling He through a 0.1 M HOCl solution [6,10] at 0 °C. The water content was further reduced by a trap held at −30 °C. CH_3OCl and C_2H_5OCl were prepared in analogy with the procedure given by Sandmeyer in 1886 [23] by passing chlorine through alkaline aqueous solutions of the corresponding alcohols. The oxychlorites were purified by repeated low-temperature distillations. i-C_3H_7OCl and tert-C_4H_9OCl were prepared using the method of Katz [24] where, on addition of dry ice to a solution of i-propanol in cold aqueous NaOCl, the equilibrium is shifted to produce the alkyl hypochlorite. Below −20 °C, the compounds are stable liquids in the dark, but they decompose above this temperature, where explosion may occur due to self-heating. Some difficulties were encountered in the handling and purification of i-propyl hypochlorite because of its relatively low vapour pressure and poor thermal stability. tert-Butyl hypochlorite is thermally stable and can be distilled even at atmospheric pressure [25].

3. Results and discussion

The simultaneous recording of the UV absorption and mass spectra under flow conditions is particularly suitable for the evaluation of absorption cross-section data. Possible contamination in the hypochlorite gas flows, e.g. decomposition products such as Cl_2, Cl_2O or the alcohols from which the hypochlorites were synthesized, can be identified mass spectrometrically and quantified.

In the carrier gas flow containing HOCl, prepared as described above [10], variable amounts of H_2O and Cl_2O were present depending on the temperature of the trap through which the gases were passed. Efficient water removal at −60 °C strongly increased the Cl_2O content [18]. With the trap kept at −30 °C, the Cl_2O/HOCl ratio was approximately 0.016. Even with the trap at 0 °C, this ratio did not drop below 0.01.

3.1. HOCl

The HOCl spectrum observed, corrected for a mass spectrometrically determined Cl_2O content of 1.2% typically present in the gas flow, is given in Fig. 1. In addition to the numerical presentation of the whole spectrum, the absorptions at λ ≥ 280 nm are given in a logarithmic presentation. In this way, the weak absorptions in the atmospherically most relevant part of the spectrum are more clearly displayed. Very good agreement is found with the spectrum reported recently by Burkholder [16]. For comparison, the spectrum reported by Permien et al. [6] is included after appropriate corrections have been applied for the presence of 17% Cl_2O. This high Cl_2O content in the samples of Permien et al. was due to the temperature of the cold trap in their experiments (−60 °C).

In Table 1, the HOCl absorption cross-sections are listed. Spectra were recorded at room temperature and at −60 °C. The absorption cross-sections for HOCl do not show noticeable differences. The cross-sections are compared with the data reported by Burkholder [16].

The continuous absorption with maxima at λ ≈ 305 and 240 nm represents the transition from the electronic ground state of the bent HOCl molecule of configuration $1^1A'$ to the

Table 1
Comparison of the UV absoption cross-sections of HOCl determined in this work with those reported by Burkholder [16]

Wavelength (nm)	Cross-section (10^{-19} cm^2 molecule^{-1})		Wavelength (nm)	Cross-section (10^{-19} cm^2 molecule^{-1})	
	This work	Ref. [16]		This work	Ref. [16]
230	1.61	1.64	312	0.59	0.57
232	1.74	1.77	314	0.57	0.56
234	1.81	1.87	316	0.55	0.54
236	1.87	1.97	318	0.52	0.51
238	1.94	2.03	320	0.50	0.49
240	2.01	2.07	322	0.48	0.46
242	2.04	2.10	324	0.46	0.43
244	2.01	2.05	326	0.43	0.42
246	1.95	1.96	328	0.39	0.38
248	1.87	1.86	330	0.37	0.35
250	1.78	1.73	332	0.34	0.33
252	1.67	1.59	334	0.31	0.31
254	1.53	1.46	336	0.27	0.27
256	1.39	1.32	338	0.26	0.25
258	1.26	1.18	340	0.23	0.24
260	1.14	1.05	342	0.20	0.21
262	1.02	0.93	344	0.17	0.18
264	0.90	0.83	346	0.15	0.18
266	0.80	0.74	348	0.14	0.17
268	0.72	0.66	350	0.13	0.15
270	0.64	0.60	352	0.12	0.13
272	0.59	0.55	354	0.11	0.13
274	0.54	0.52	356	0.10	0.12
276	0.51	0.49	358	0.08	0.10
278	0.49	0.48	360	0.07	0.08
280	0.48	0.47	362	0.06	0.10
282	0.47	0.48	364	0.05	0.10
284	0.48	0.48	366	0.04	0.09
286	0.50	0.49	368	0.03	0.08
288	0.52	0.51	370	0.03	0.08
290	0.54	0.53	372	0.02	0.10
292	0.55	0.54	374	0.01	0.08
294	0.57	0.56	376	0.02	0.08
296	0.58	0.58	378	0.03	0.06
298	0.59	0.59	380	0.03	0.08
300	0.60	0.60	382	0.03	
302	0.60	0.60	384	0.02	
304	0.61	0.61	386	0.02	
306	0.61	0.60	388	0.01	
308	0.62	0.60	390	0.02	
310	0.61	0.59	392	0.01	

lowest lying states $1^1A''$ and $2^1A'$ [26,27]. These Renner–Teller split paired states corresponding to the linear $^1\Pi$ configuration of excited HOCl are slightly bent and linear respectively. Light absorption in this spectral region will lead to a direct dissociation of the HOCl molecule into OH($^2\Pi$) and Cl(^{2}P) radicals. No other channel is available in this wavelength range, but excitation energy affects the state distribution of the dissociation products. No information on spin–orbit coupling can be obtained directly from the available ab initio calculations.

In agreement with these considerations, HOCl photodecomposes on irradiation in this wavelength region with a quantum yield of unity [10] and OH and Cl radicals are

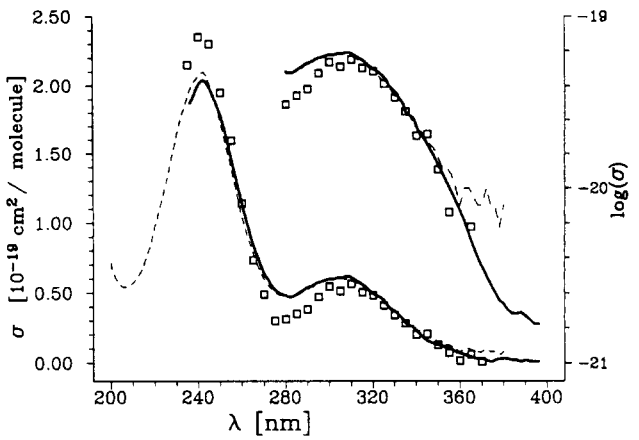

Fig. 1. Comparison of the UV absorption spectrum of HOCl determined in this work (full line) with the spectra reported by Burkholder [16] (broken line) and Permien et al. [6] corrected for Cl_2O contributions (squares). For a clearer display of the weak absorptions, the long-wavelength part of the spectrum is also presented using the logarithmic scale on the right-hand side.

positively identified as intermediates [7,10]. The analysis of the state distributions in the photofragments OH and Cl, as monitored by laser-induced fluorescence (LIF) [9,11] and resonantly enhanced multiphoton ionization (REMPI) experiments [12], has been reported. Recent laser photolysis experiments with REMPI mass spectrometry (MS) detection of the photofragments [28] lend further support to this assignment.

Most gratifying is the excellent agreement of two recent quantum mechanical calculations of the vertical excitation energy in HOCl [26,27] with our experimental absorption data. Nambu and Iwata [26] reported, for the states $1^1A''$ and $2^1A'$ calculated energies of 4.02 and 5.16 eV. The experimental absorption maxima at $\lambda = 305$ and 240 nm correspond to excitation energies of 4.06 and 5.16 eV. In earlier calculations, the lowest lying excited states in HOCl were reported to be at 4.54 and 5.75 eV [29].

3.2. CH_3OCl

The simultaneously recorded UV absorption and mass spectra of CH_3OCl revealed that samples prepared under seemingly identical conditions contained up to 5 vol.% CH_3OH and varying amounts of Cl_2 (always less than 2 vol.%). Information on the CH_3OH and Cl_2 contents in the sample is needed for absorption cross-section data evaluation. Knowledge of the Cl_2 content of the samples was of particular importance in photolysis experiments at $\lambda = 308$ nm carried out recently (see below) [28].

The absorption spectrum of CH_3OCl is given in Fig. 2. Again, in addition to a numerical presentation of the whole spectrum in the range 200 nm $< \lambda <$ 450 nm, for $\lambda \geqslant 280$ nm a logarithmic display of the weak absorptions is included. The cross-sections in Table 2 represent the data from samples in which the CH_3OH content was less than 1%. The spectrum was corrected for a Cl_2 content of 0.5%. The difference between the uncorrected and corrected absorptions in the

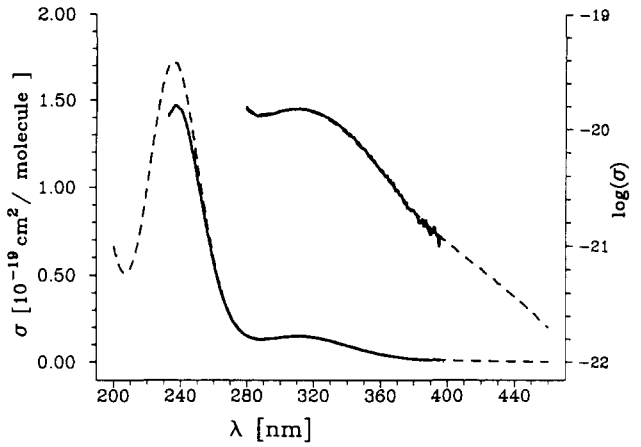

Fig. 2. UV absorption spectra of CH_3OCl determined in this work (full line) and by Crowley et al. [30] (broken line). For the logarithmic scale, see Fig. 1.

range 300 nm < λ < 400 nm is shown in Fig. 3. Cross-sections obtained from measurements at room temperature and at −60 °C showed no noticeable differences. At the time of carrying out these experiments, no other absorption data for CH_3OCl were available in the literature. Very recently, the results of an investigation from another group have become available [30]. These data are included for comparison in Figs. 2 and 3 as well as in Table 2.

As for HOCl, the long-wavelength continuous absorption of CH_3OCl shows a distinct maximum at λ = 235 nm and another flat maximum at λ = 308 nm. No detailed theoretical studies are available, at present, on the potential energy surfaces of the electronic ground and excited states of CH_3OCl which could be related to the experimentally observed photoabsorptions. However, based on the evident similarity in the absorption properties of HOCl and CH_3OCl in this wavelength range, which suggests that the substitution of the hydrogen atom by a methyl group does not affect the electronic configuration substantially in the chromophore, it is proposed that both maxima belong to one set of paired states comparable with the situation in HOCl [26]. Consequently, the photolysis of CH_3OCl in this range should lead to the products $CH_3O(^2E)$ and $Cl(^2P)$ only. Changes in the excitation energy may alter the state distribution in the dissociation products.

At present, no report exists in the literature on the photolysis of CH_3OCl in the gas phase. Sets of experiments on the laser-induced decomposition of CH_3OCl at λ = 308 nm and 237–245 nm carried out in this laboratory [28] revealed that Cl atoms are produced during photolysis with a quantum yield very close to unity. The atoms are identified to be generated in the states $^2P_{3/2}$ and $^2P_{1/2}$, the ratio being a function of the excitation energy. Also, the generation of ClO radicals in the photolytic decomposition of CH_3OCl can be clearly excluded on the basis of REMPI MS analysis results [28].

In addition to absorption spectroscopy, mass spectrometry can be employed in kinetic studies of the involvement of CH_3OCl in atmospheric oxidation cycles. As a supplement to the absorption data, the electron impact mass spectrum of CH_3OCl is presented in Fig. 4. It possesses characteristic parent ion base signals as well as strong $(M-1)^+$ ions. Calibrations have shown that detection limits in the region of 10^8 molecules cm^{-3} can be reached for this oxychloride in flow experiments.

The IR spectrum of CH_3OCl, given in Fig. 5, shows only a very weak absorption in the OCl stretching band range (see below). This can be related to small dipole moment changes on stretching of this bond. Ab initio frequency calculations at the Hartree–Fock (HF) level of theory were carried out with a 6-31G(p) basis set using the GAUSSIAN 92 program

Table 2
Comparison of the UV absorption cross-sections of CH_3OCl determined in this work with those given by Crowley et al. [30]

Wavelength (nm)	Cross-section (10^{-19} cm^2 $molecule^{-1}$)		Wavelength (nm)	Cross-section (10^{-19} cm^2 $molecule^{-1}$)	
	This work	Ref. [30]		This work	Ref. [30]
230	1.37	1.61	314	0.148	0.147
232	1.40	1.68	316	0.148	0.145
234	1.43	1.72	318	0.145	0.142
236	1.46	1.72	320	0.143	0.139
238	1.46	1.71	322	0.139	0.136
240	1.45	1.66	324	0.135	0.132
242	1.40	1.59	326	0.132	0.128
244	1.34	1.50	328	0.126	0.123
246	1.26	1.39	330	0.122	0.118
248	1.17	1.28	332	0.116	0.113
250	1.07	1.15	334	0.111	0.107
252	0.962	1.03	336	0.106	0.102
254	0.859	0.913	338	0.0997	0.0964
256	0.755	0.800	340	0.0929	0.0908
258	0.664	0.696	342	0.0897	0.0853
260	0.574	0.600	344	0.0844	0.0800
262	0.495	0.515	346	0.0773	0.0748
264	0.423	0.440	348	0.0721	0.0697
266	0.362	0.376	350	0.0676	0.0649
268	0.311	0.322	352	0.0621	0.0602
270	0.267	0.275	353	0.0591	0.00558
272	0.231	0.239	356	0.0541	0.0517
274	0.202	0.211	358	0.0486	0.0478
276	0.180	0.186	360	0.449	0.0441
278	0.161	0.168	362	0.0415	0.0408
280	0.150	0.156	364	0.0403	0.0376
282	0.140	0.145	366	0.0365	0.0347
284	0.135	0.140	368	0.0341	0.0321
286	0.130	0.136	370	0.0301	0.0296
288	0.131	0.134	372	0.0273	0.0274
290	0.130	0.135	374	0.0239	0.0253
292	0.132	0.136	376	0.0215	0.0235
294	0.134	0.137	378	0.0201	0.0218
296	0.136	0.139	380	0.0201	0.0203
298	0.138	0.142	382	0.0185	0.0188
300	0.142	0.144	384	0.016	0.0175
302	0.145	0.145	386	0.0151	0.0164
304	0.146	0.148	388	0.015	0.0154
306	0.148	0.149	390	0.0126	0.0144
308	0.149	0.149	392	0.0139	0.0135
310	0.149	0.149	394	0.0124	0.0127
312	0.149	0.148			

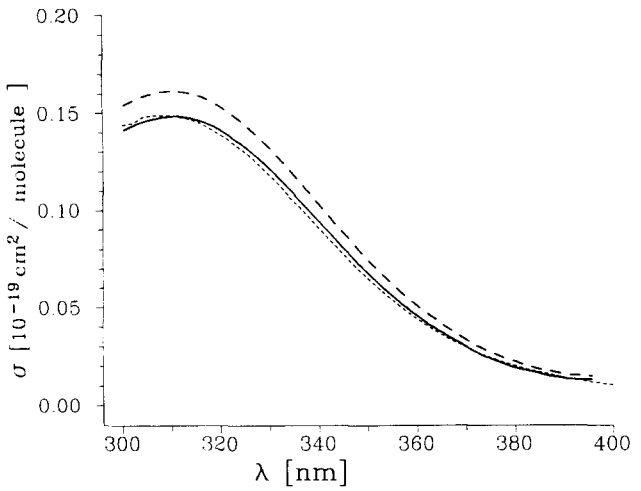

Fig. 3. A comparison of the CH_3OCl data in the range 300–400 nm: measured absorption (broken line); absorption corrected for mass spectrometrically determined 0.5% Cl_2 content (full line); cross-section data from Ref. [30] (dotted line).

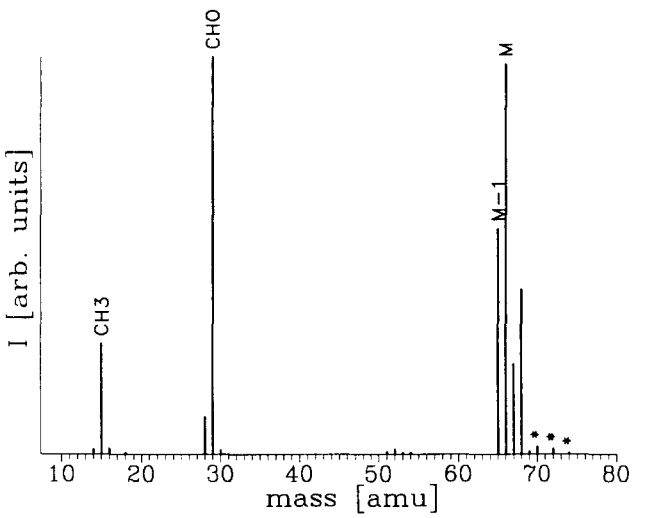

Fig. 4. Electron impact mass spectrum of CH_3OCl recorded at 30 eV. Signals due to 0.5% Cl_2 impurity are marked.

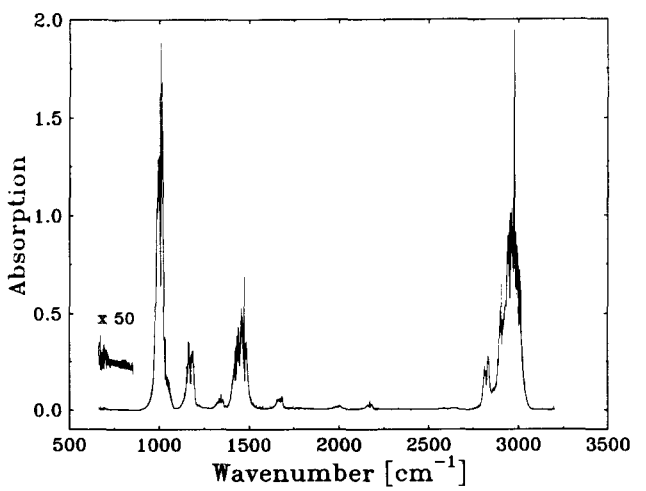

Fig. 5. Fourier transform IR spectrum of CH_3OCl.

package [31]. Calculated frequencies, scaled by 0.89, and intensity ratios agree quite well with the experimental data (Table 3). The bands near 1675 and 2170 cm^{-1} were not assigned, but seem to be a spectral feature of CH_3OCl.

The stability of the CH_3OCl samples in the absorption cell was checked by following the gradual deterioration of the spectrum of a freshly prepared sample standing in the cell at room temperature at 0.5 mbar. After several hours, the CH_3OCl spectrum disappeared and absorptions of methanol, formaldehyde, HCl and CO_2 were registered.

3.3. C_2H_5OCl, i-C_3H_7OCl and tert-C_4H_9OCl

Corrected absorption spectra for these alkyl hypochlorites at 230 nm < λ < 400 nm are compiled in Fig. 6. The difficulties encountered in the preparation and purification of C_2H_5OCl and i-C_3H_7OCl as well as their limited stability are reflected in an estimated impurity level of 10%–20% based on mass spectrometric analysis. Interference resulted predominantly from fragments of the alcohols from which the hypochlorites were synthesized and decomposition products

Table 3
Comparison of the calculated and experimentally observed vibrational frequencies of CH_3OCl together with their assignement. Normal mode frequencies ν in cm^{-1}; intensities in debye^2 $Å^{-2}$ amu^{-1}

Calculated ν	Experimental ν	Assignment
295 (3.4)		CH_3 torsion
404 (2.4)		δ (C–O–Cl)
701 (7.4)	≈680 (vw)	ν (Cl–O)
1037 (88.1)	1002 (s)	ν (C–O)
1146 (3.5)	1150 (w)	δ (C–H) rocking
1177 (11.9)	1170 (m)	δ (C–H) rocking
1436 (15.1)	1424 (m)	δ (C–H) antisymm.
1449 (5.0)	1456 (m)	δ (C–H) umbrella
1474 (9.7)	1471 (m)	δ (C–H) scissoring
2869 (40.9)	2820 (s)	ν (C–H) symm.
2939 (45.4)	2904 (s)	ν (CH–H) antisymm.
2959 (19.5)	≈2920 (m)	ν (C–H) antisymm.

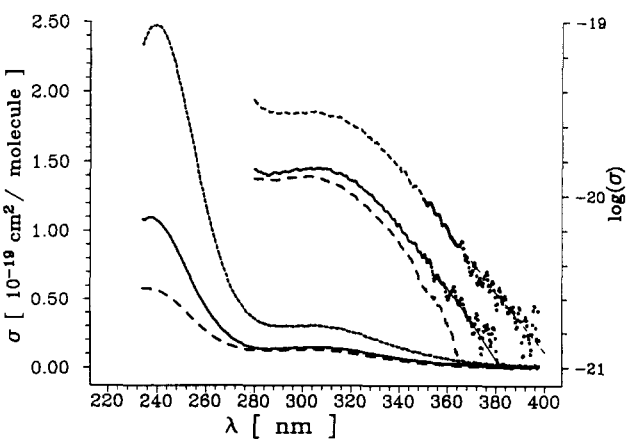

Fig. 6. UV absorption cross-sections of ROCl: R ≡ C_2H_5 (full line), i-C_3H_7 (broken line), tert-C_4H_9 (dotted line). For the logarithmic scale, see Fig. 1.

(see IR data above). Thus the cross- section data represent the lower limits with a possible error of up to 20%.

Acknowledgements

This work was supported in part by the BMFT, Bonn, within contract 01 LO 9103. T.P.W.J. and U.K. acknowledge the "Promotions-stipendium des Landes Schleswig-Holstein". The authors are obliged to Dr. J.N. Crowley for making data available prior to publication.

References

[1] J.P.D. Abbatt and M.J. Molina, *J. Phys. Chem., 96* (1992) 7674.
[2] B. Reimann and F. Kaufmann, *J. Chem. Phys., 69* (1978) 2925.
[3] L.T. Molina and M.J. Molina, *J. Phys. Chem., 82* (1978) 2410.
[4] H.-D. Knauth, H. Alberti and H. Clausen, *J. Phys. Chem., 83* (1979) 1604.
[5] E.A. Mishalanie, C.J. Rutkowski, R.S. Hutte and J.W. Birks, *J. Phys. Chem., 90* (1986) 5578.
[6] T.R. Permien, R. Vogt and R.N. Schindler, *Air Pollution Rep. 17*, Environ. Res. Progr. CEC, Brussels, 1988.
[7] M.J. Molina, T. Ishiwata and L.T. Molina, *J. Phys. Chem., 84* (1980) 821.
[8] P.J. Butler and L.F. Phillips, *J. Phys. Chem., 87* (1983) 183.
[9] A.J. Bell, P.R. Pardon, C.G. Hickman and J.G. Frey, *J. Chem. Soc., Faraday Trans., 86* (1990) 3831.
[10] R. Vogt and R.N. Schindler, *J. Photochem. Photobiol. A: Chem., 66* (1992) 133.
[11] C.G. Hickman, N. Shaw, M.C. Crawford, A.J. Bell and J.G. Frey, *J. Chem. Soc., Faraday Trans., 89* (1993) 1623.
[12] A.J. Bell, S.A. Boggis, J.M. Dyke, J.G. Frey, R. Richter, N. Shaw and M. Tabrizchi, *J. Chem. Soc., Faraday Trans., 90* (1994) 17.
[13] J.L. Cook, C.A. Ennis, T.J. Leck and J.W. Birks, *J. Chem. Phys., 74* (1981) 545.
[14] K.V. Chance, D.G. Johnson and W.A. Traub, *J. Geophys. Res., 94* (1989) 11 059.
[15] G.C. Toon and C.B. Farmer, *Geophys. Res. Lett., 16* (1989) 1375.
[16] J.B. Burkholder, *J. Geophys. Res., 98* (1993) 2963.
[17] R. Vogt and R.N. Schindler, *Geophys. Res. Lett., 19* (1992) 1935.
[18] R. Vogt and R.N. Schindler, *Ber. Bunsenges. Phys. Chem., 97* (1993) 819.
[19] P.J. Crutzen, R. Müller, Ch. Brühl and Th. Peter, *Geophys. Res. Lett., 19* (1992) 1113.
[20] F. Helleis, J.N. Crowley and G.K. Moortgat, *J. Phys. Chem., 97* (1993) 11 464.
[21] R.D. Kenner, K.R. Ryan and I.C. Plumb, *Geophys. Res. Lett., 20* (1993) 1571.
[22] A.S. Kukui, T.P.W. Jungkamp and R.N. Schindler, *Ber. Bunsenges. Phys. Chem., 98* (1994) 1298.
[23] T. Sandmeyer, *Ber. Deutsche Chem. Ges., 19-I* (1886) 857.
[24] I. Katz, *A.P. 2 694 722*, Bjorksten Res. Lab., 1954.
[25] F.D. Chattaway and O.G. Backeberg, *J. Chem. Soc., 123* (1923) 2999.
[26] S. Nanbu and S. Iwata, *J. Phys. Chem., 96* (1992) 2103.
[27] H. Guo, *J. Phys. Chem., 97* (1993) 2602.
[28] M. Liesner, Th. Benter, U. Kirchner and R.N. Schindler, in preparation.
[29] P.J. Bruna, G. Hirsch, S.D. Peyerimhoff and R. Buenker, *Can. J. Chem., 57* (1979) 1839.
[30] J.N. Crowley, F. Helleis, R. Müller, K.G. Moortgat, P.J. Crutzen and J.J. Orlando, *J. Geophys. Res., 99* (1994) 20 683.
[31] M.J. Frisch, G.W. Trucks, M. Head-Gordon, P.M.W. Gill, M.W. Wong, J.B. Foresman, B.G. Johnson, H.B. Schlegel, M.A. Robb, E.S. Replogle, R. Gomperts, J.L. Andres, K. Raghavachari, J.S. Binkley, C. Gonzalez, R.L. Martin, D.J. Fox, D.J. Defrees, J. Baker, J.J.P. Stewart and J.A. Pople, *Gaussian 92*, Revision C, Gaussian, Inc., Pittsburgh, PA, 1992.